A simultaneous operando FTIR & Raman study of propane ODH mechanism over V-Zr-O catalysts

J.J. Ternero-Hidalgo, M. Daturi, Guillaume Clet, P. Bazin, M.A. Bañares, R. Portela, M.O. Guerrero-Pérez, J. Rodríguez-Mirasol, T. Cordero

A simultaneous *operando* FTIR & Raman study of propane ODH mechanism over V-Zr-O catalysts

J. J. Ternero-Hidalgo[1], M. Daturi[2*], G. Clet[2], P. Bazin[2], M. A. Bañares[3], R. Portela[3], M.O. Guerrero-Pérez[1*], J. Rodríguez-Mirasol[1], T. Cordero[1*]

[1] *Universidad de Málaga, Departamento de Ingeniería Química, E29071 Málaga, Spain*
[2] *Normandie Univ, ENSICAEN, UNICAEN, CNRS, LCS, 14000 Caen, France*
[3] *Instituto de Catálisis y Petroleoquímica, CSIC, E28049 Madrid, Spain*

Keywords: propane ODH; reaction mechanism; active sites; structure-activity relationships; *operando* IR-Raman;

Abstract: Simultaneous *operando* Raman and transmission FTIR spectroscopic measurements have been combined for the study of the structure-activity relationships of V-Zr-O catalysts during propane oxidative dehydrogenation (ODH). The combination of both spectroscopies during reaction allows the identification of reaction intermediates and yields structural information about the catalyst. The experimental results are compared with available data in the literature to propose a reaction mechanism for propane ODH on V-Zr-O catalytic systems, and to identify the role of different oxygen species bound to vanadium sites. The results are consistent with a Mars-van Krevelen mechanism. Besides, they clearly show higher activity of bridging oxygen sites (V-O-V, V-O-Zr) than terminal V=O bonds.

1. Introduction

The catalytic selective oxidation of hydrocarbons [1,2] is a strategic route to produce value-added chemicals. Among these processes, the oxidative dehydrogenation (ODH) of propane to obtain propylene has been extensively studied over the past decades [3–5], since propylene has become the second most-demanded building block (after ethylene) in the petrochemical industry [6,7]. However, the low propylene yields obtained by propane ODH have hindered its industrial implementation [3]. The non-oxidative dehydrogenation reaction is therefore practiced in the industry [8], although it is an energy-intensive process with several hurdles that may be solved with the ODH route [4,5].

Catalysts based on dispersed vanadia species over different supports (ZrO_2, TiO_2, Al_2O_3, SiO_2, etc.) are highly reported in literature for propane ODH [3,4,9–12]. It has been established that the reaction proceeds via Mars-van-Krevelen type mechanism [4,5,13–19], which involves the sequential reduction and reoxidation of the catalyst surface by reaction with, respectively, propane and oxygen (or other oxidizing agents, like N_2O [14,20]). The generally accepted reaction network is a parallel-consecutive pathway, where propane is oxidized to propylene, and both can be totally oxidized to CO_x [5,21]. Moreover, it is commonly reported that it is difficult to control such undesired combustion to CO_x, which lowers propylene yields, because the same lattice oxygen active sites are responsible for both selective and total oxidation, and propylene activation requires lower energy with respect to propane [4,5,22,23].

There is a debate on the propylene formation mechanism, but there are even less details about the nature and number of steps that lead to CO_x formation [5]. It is accepted that the first proton abstraction from propane is the rate-determining step; however, the low coverage and short lifetime of subsequent intermediates limit their detection by traditional transient or steady-state methods. Iglesia *et al*. carried out isotopic tracer studies to investigate the propane ODH reaction mechanism over VO_x/ZrO_2 catalysts [24,25]. The results suggested that propane is most probably attacked at C(2), the weakest C-H bond, forming isopropoxide species, and that both propane C-H bond activation and dissociative oxygen chemisorption (to reoxidize the catalyst) are irreversible steps, while the -OH groups formed during reaction on the catalyst reversibly recombine into water, creating oxygen active sites and vacancy centers. Ultra-rapid FTIR analysis coupled with MS during propane oxidation on a V-based catalyst demonstrated that oxygenates are not formed during the first minutes of reaction, showing that propylene is formed directly from propane via dehydrogenation on a V-O site [26]. As observed for spinel-type catalysts (Co_3O_4, Mn_3O_4 and $MgCr_2O_4$) [27], the hydrocarbon species may evolve to propylene (acid-basic elimination step) or to chemisorbed acetone (redox step). The latter is more easily overoxidized to CO_x through acetate and formate species as intermediates, with the consequent formation of carbonates.

Regarding active sites, since 1968 terminal V=O bonds have been proposed as the most active site [28–37]. However, since the 1990s, other authors have reported experimental evidence that the vanadyl bond is hardly reactive and that the bridging oxygens (V-O-V/V-O-support) are the catalytic active sites for selective oxidation reactions [4,38–65]. Several *in situ* and *operando* IR, Raman and UV-Vis DRS

spectroscopy studies (some of them including $^{18}O_2/^{16}O_2$ isotopic labeling) provide experimental evidence of the non-involvement of the terminal vanadyl oxygens and of the key role of the bridging V-O-support bonds in the kinetic rate determining step [4,38,52–65]. Furthermore, Bañares *et al*. have shown independence [66] and even opposite [67] correlation between the V=O bond strength and alkane ODH reactivity.

The aim of the present paper is to uncover the role of the different oxygen sites and the propane ODH mechanism over V-Zr-O catalysts. A new homemade *operando* IR-Raman cell [68], designed in a joint CSIC-LCS collaboration, is used to obtain in a single *operando* experiment information about the structure of the catalyst (Raman and infrared), the adsorbed species (mainly, but not only, from FTIR), and the reactivity (online gas measurement) during reaction. This combination offers a higher possibility to directly connect relevant details about the structure-activity relationships of the catalyst-reactants interplay during reaction.

2. Experimental

2.1. Catalysts preparation

The preparation of the catalysts by electrospinning is described elsewhere [69]; zirconium (IV) propoxide, polyvinylpyrrolidone (PVP), acetylacetone, 1-propanol and vanadyl acetylacetonate were the precursors. Polymer solutions were prepared by mixing the precursors in adequate amounts to obtain final fibers with nominal concentration of elemental vanadium of 2.5 wt. % (Zr-V2.5), 5.0 wt. % (Zr-V5.0) and 6.4 wt. % (Zr-V6.4). These polymer solutions were vigorously stirred at room temperature for 24 h before the electrospinning process, as described in previous articles [69,70]. The electrospun fibers were calcined in air flow (150 mL·min^{-1} STP)

at 500ºC (10 ºC·min^{-1} heating rate) for 6 h. XPS analyses of the final catalysts Zr-V2.5, Zr-V5.0 and Zr-V6.4 indicate surface mass concentrations of elemental vanadium of 2.7, 4.9 and 6.0 %, respectively, as published in a previous work [69].

2.2. *Characterization*

X-ray diffraction patterns (XRD) were acquired in the region of 2Θ=5–80° for 30 min on an EMPYREAN diffractometer of PANalytical using CuKα1,2 (1.5406 Å) monochromatic radiation (operational value 45 kV and 40 mA), a detector PIXcel and Soller slits (incident and diffracted beam) of 0.04 rad.

X-ray photoelectron spectroscopy (XPS) analyses of the catalysts were obtained by a 5700C model Physical Electronics apparatus with MgKα radiation (1253.6 eV). The maximum of the C1s peak was set at 284.5 eV and used as a reference to shift the other peaks.

2.3. *ODH reaction in IRRaman operando reactor*

Scheme 1 represents the *IRRaman operando* reactor, which is an evolution, developed in collaboration with CSIC, of the IR “sandwich” catalysis cell designed at LCS [71]. The cell is placed in the bench of a Nicolet 6700 FT-IR spectrometer (64 scans/spectrum) equipped with a MCT/A detector that allows direct acquisition of transmission IR spectra. For Raman measurements, the laser beam (532 nm) is brought to the sample in the catalysis cell via an *ad hoc* InPhotonics Raman probe specially designed to withstand high temperatures. The Raman signal was obtained using low power (5 mW) to prevent local heating and analysed by a Horiba Jobin Yvon Labram300 spectrometer. The dual IR-Raman *operando* reactor can be fed with different controlled gas flows and a capillary thermocouple was placed on the

sample for temperature control. Downstream the reactor, the exhaust gases are simultaneously measured using an IR gas cell and a mass spectrometer. The lines were heated to 60 ºC to pre-heat the reactant mixture and avoid product condensation. Complete information on this cell is provided elsewhere [68].

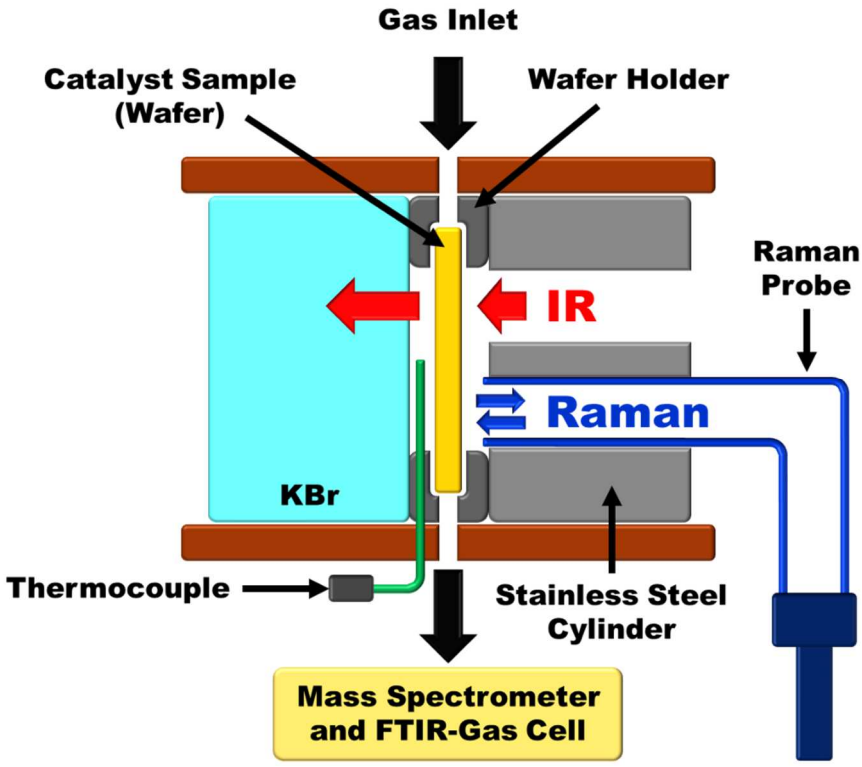

Scheme 1. Conceptual representation of the IRRaman *operando* reactor.

The structured fiber catalysts were grinded and pressed into self-supported wafers to perform the catalytic experiments in a reactor-cell behaving as a plug flow reactor, as already calculated [72]. As described previously, wafers were made with pressures below 1 ton/cm^2 to preserve adequate porosity to prevent diffusion control phenomena [73]. The weight of catalyst wafer (W_{cat}) and the total volumetric gas flow (F_T) were fixed to 31.5 mg and 18.1 mL·min^{-1}, respectively. The reaction temperature ranged from 200 to 340 ºC. Oxidation was performed with 10% oxygen in argon,

while reaction was performed with 20% propane and 10% oxygen in argon (ODH conditions) or 20% propane in argon (DH conditions). The samples were first dehydrated at 340ºC (5ºC·min^{-1}) in 10% O_2/Argon. After this activation step, the experiments were run at 200, 250, 300 and 340 ºC, switching at each temperature between four different conditions in the following order: ODH reaction, oxidation, DH reaction, and oxidation. The conditions were changed after achieving steady or quasi-steady state. A propylene ODH experiment was also performed in order to obtain more mechanistic information about the consecutive total oxidation of propylene to CO_x.

FTIR and Raman *operando* spectra of the catalysts were acquired every 2 and 4 min, respectively, with an acquisition time of 39 s for the former and typically 180 s for the latter. Online gas-phase FTIR and MS spectra were collected every 2 min and 3 s, respectively. In all experiments the carbon molar balances were attained with a maximum error of 5%. Propane or oxygen conversion ($X_{C_3H_8}$ or X_{O_2}, respectively) and the selectivity to *i* product (S_i) were defined as:

$$X_i(\%) = \frac{\dot{F}_{o,i} - \dot{F}_i}{\dot{F}_{o,i}} 100 \quad (1)$$

$$S_i(\%) = \frac{n_i \dot{F}_i}{n_{C_3H_8} \dot{F}_{0,C_3H_8} X_{C_3H_8}} 100 \quad (2)$$

where $\dot{F}_{o,i}$ and $\dot{F}_i$ are the molar flows of reactant/product "*i*" in the inlet and in the outlet streams, respectively, and n_i is the number of carbon atoms in molecule *i* (n_{C3H8} = 3). Turn-over frequency (TOF) describes the specific activity and was calculated from Eq. (3); it quantifies the moles of propane converted per mol of vanadium and unit time:

$$TOF = \frac{\dot{F}_{0,C_3H_8} X_{C_3H_8} M_V}{W_{cat} W_V} \quad (3)$$

where M_V denotes the molar mass of vanadium and W_V the mass of vanadium per gram of catalyst. This parameter assumes that all the active sites are exposed to the reactants, have the same catalytic activity and are stable during the reaction. The first assumption is supported by the Raman spectra showing that all vanadia is present as molecularly dispersed surface vanadium oxide (Figure 1). There is no evidence of bulk species like ZrV_2O_7 (Raman bands at 900, 780 cm^{-1}) [74–76], or crystalline V_2O_5 (Raman bands at 143 and 994 cm^{-1}) [77], which rules out TOF overestimation due to trapped vanadia.

In order to discard a possible contribution of the homogeneous gas phase reaction and/or of the zirconia support to the catalytic results of propane ODH, blank experiments were run without catalyst and with a vanadium-free zirconia sample. In both cases, propane conversion values were negligible. The possible influence of the Raman laser on the catalytic activity was checked by performing FTIR *operando* experiments with and without the Raman and no significant differences were found.

Moreover, the samples were examined after the *operando* experiments and no dark spots due to the laser incidence were observed. This suggests that hotter zones, where coke could preferentially form, did not occur during reaction.

3. Results and Discussion

3.1. *Fresh catalysts characterization*

Figure 1 shows the simultaneous Raman (Figure 1, green) and infrared (Figure 1, red) spectra of the dehydrated Zr-V5.0 catalyst at 340ºC. The characteristic Raman bands of zirconia tetragonal phase observed at 642, 459, 314 and 268 cm^{-1} [69,78] are consistent with the XRD patterns (Figure S1 in Supplementary information). XRD peaks of zirconia support become smaller and broader with vanadia loading. When these materials are prepared using the strategy of one-pot synthesis, the dispersed components tend to hinder the growth and sintering of crystallites and phase transformation of the support resulting in smaller and more amorphous of ZrO_2 crystallites [79]. The broadest Raman signal corresponds to V-O-V (ca. 880 cm^{-1}) and V-O-Zr in ZrV_2O_7 -like structure (770 cm^{-1}) [39,58,69,77]. Raman and infrared spectra show the 1020 cm^{-1} V=O mode of molecularly dispersed vanadium oxide species [58,74,76]. The presence of crystalline V_2O_5 can be excluded, since its characteristic Raman bands at 143 and 994 cm^{-1} are absent [77]. These results are also consistent with the V $2p_{3/2}$ XPS spectra (Figure S2 in Supplementary information), which binding energy values do not correspond to bulk V_2O_5 (517.2 eV) [80]; thus underlining the interaction between molecularly dispersed vanadia and ZrO2. Moreover, some weak infrared bands around 3700 cm^{-1} are apparent due to the hydroxyl groups. The infrared bands in the range of 1300-1600 cm^{-1} can be attributed to carbonaceous deposits [81,82] and carbonate species [83]; which may

come from the decomposition during calcination of the carbonaceous precursors and polymer used for the preparation of the different catalysts. The sharp band near 2339 cm^{-1} is associated with occluded CO_2 [84,85].

The other two catalysts, Zr-V2.4 and Zr-V6.4, presented very similar Raman and infrared features; as expected, the intensity of the vanadium oxide bands increased and the V=O mode blue-shifted with increasing vanadium oxide loading [68]. This shift is due to a higher relative population of polyvanadates with respect to monovonadates in catalysts with higher vanadium contents [86]. With respect to the bands related with the carbonaceous deposits and carbonate species, the intensity increases as the vanadia content decreases; this would be associated with the capacity of vanadia to catalyze the decomposition of these carbonaceous species during the calcination.

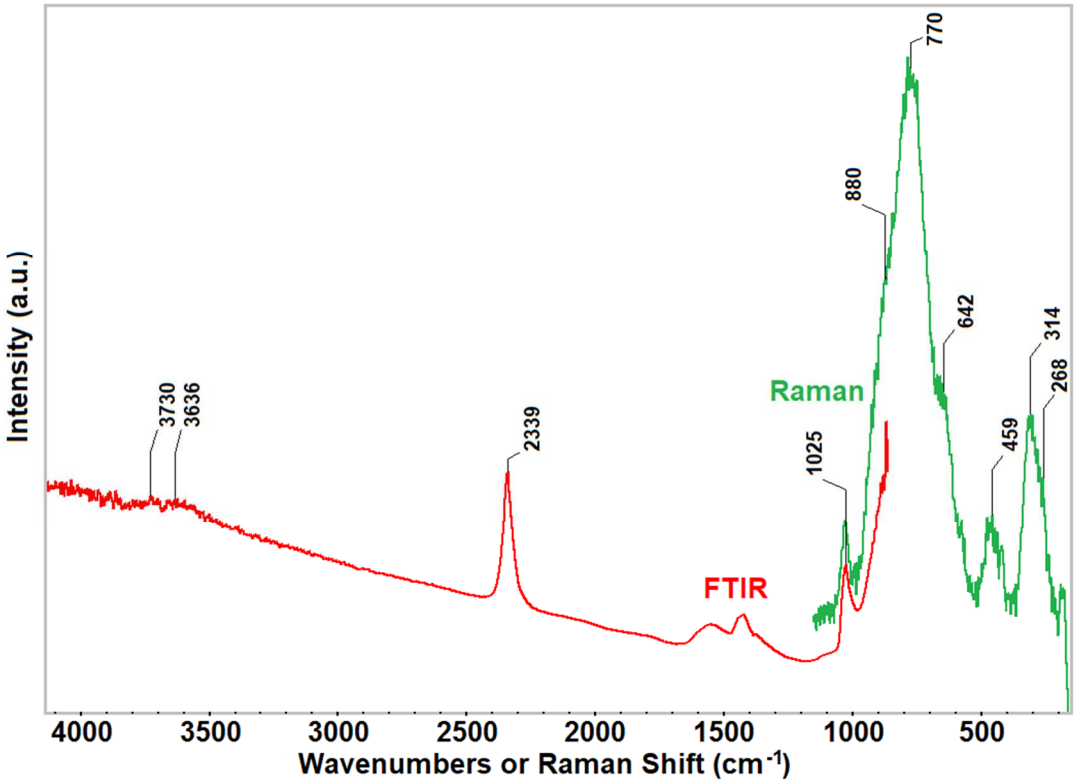

Figure 1. Raman (green) and FTIR (red) spectra obtained for the Zr-V5.0 catalyst in the IRRaman *operando* reactor under activation flow (10% O_2 in Ar) at 340ºC.

3.2. *Operando* characterization *during reaction*

3.2.1. Propane ODH

The activity results obtained during propane ODH *operando* experiments in the IRRaman reactor are shown in Table 1. Propane conversion is apparent at 250ºC for Zr-V6.4 and Zr-V5.0 and at 300ºC for Zr-V2.5. The conversion and TOF values increase with vanadium loading, suggesting some higher reactivity of polymeric vanadium sites. These data are consistent with previous data of these catalysts in a conventional plug-flow reactor [69].

Table 1. ODH activity results obtained during the *operando* experiments in the IRRaman reactor (catalyst weight: 31.5 mg, total flow: 18.1 mL/min). The results obtained in a conventional fixed-bed reactor with a space-time of 0.6 $g \cdot s \cdot mL^{-1}_{C3H8}$ at 300ºC are from Ref. [69].

Temperature (ºC)	Catalyst	X_{C3H8} (%)	X_{O2} (%)	S_{C3H6} (%)	S_{COx} (%)	Y_{C3H6} (%)	$TOF^{a} \cdot 10^3$ (s^{-1})
200	Zr-V2.5	0	0	0	0	0	0
	Zr-V5.0	0	0	0	0	0	0
	Zr-V6.4	0	0	0	0	0	0
250	Zr-V2.5	0	0	0	0	0	0
	Zr-V5.0	0.6	0.7	78.8	21.2	0.47	0.51
	Zr-V6.4	0.9	1.3	82.0	18.0	0.74	0.63
300	Zr-V2.5	0.7	1.3	82.8	17.2	0.58	1.09
	Zr-V5.0	1.6	3.5	74.5	25.5	1.19	1.37
	Zr-V6.4	2.1	5.9	68.3	31.7	1.43	1.47
300 (conventional fixed-bed reactor)	Zr-V5.0	1.9	4.6	76.9	23.1	1.46	1.63
340	Zr-V2.5	1.3	6.6	71.4	28.6	0.93	2.02
	Zr-V5.0	3.2	10.9	75.8	24.2	2.42	2.74
	Zr-V6.4	5.3	24.3	58.5	41.5	3.10	3.71

[a] TOF based on XPS analyses.

Figure 2 presents the FTIR and Raman *operando* spectra obtained during propane ODH and DH (green and yellow traces, respectively) along with dehydrated state before and after reaction (blue and pink traces, respectively) at different

temperatures for Zr-V2.5, Zr-V5.0 and Zr-V6.4 (Figure 2 A, B and C, respectively). The FTIR spectra are shown in the 1750-1100 cm^{-1} range (subtracted spectra to show adsorbed species; Figure 2 A1, B1 and C1), and the 1100-900 cm^{-1} range (full spectra showing the vanadia species; Figure 2 A2, B2 and C2). The Raman spectra are presented in the region 1100-525 cm^{-1} (Figure 2 A2, B2 and C2).

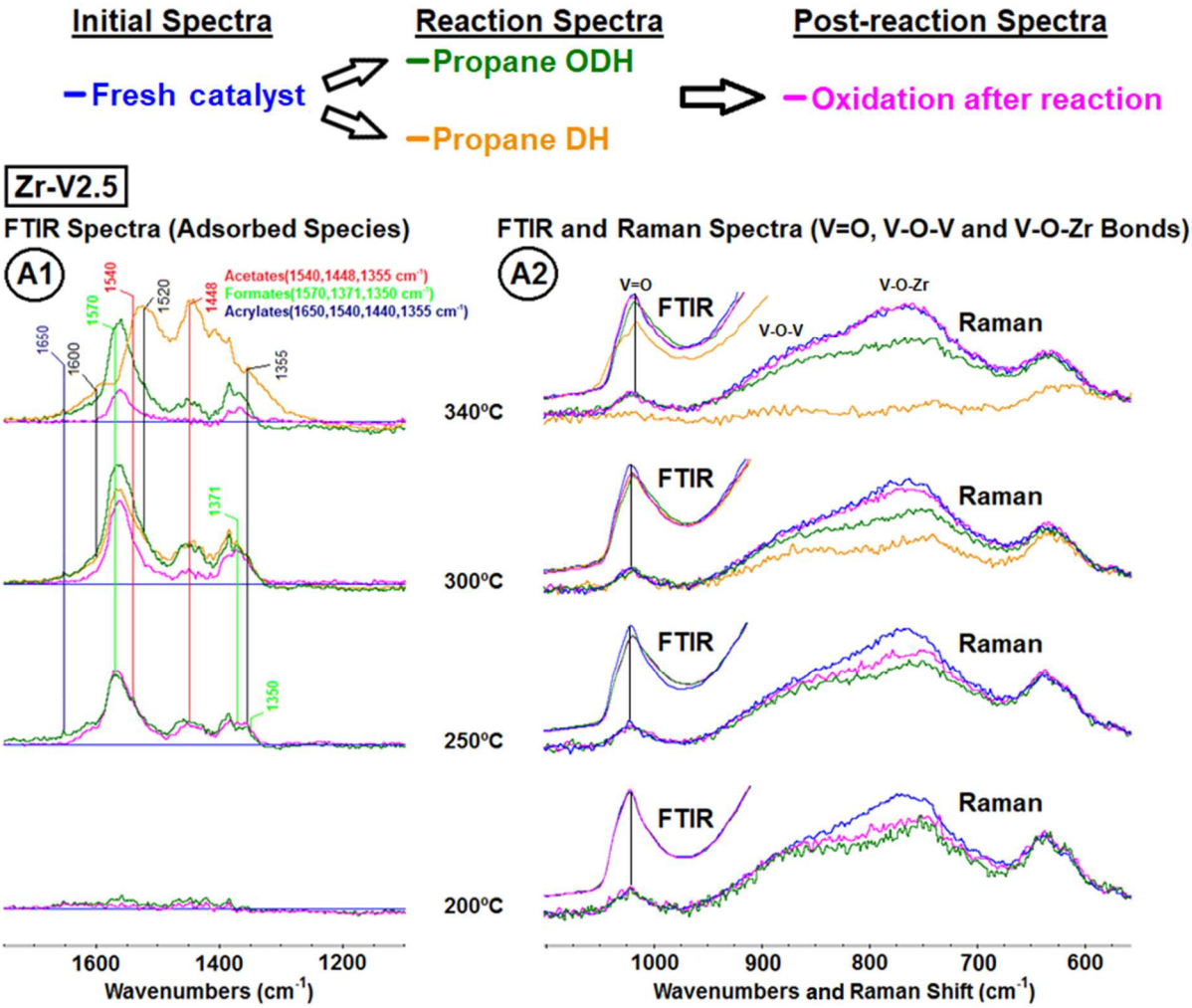

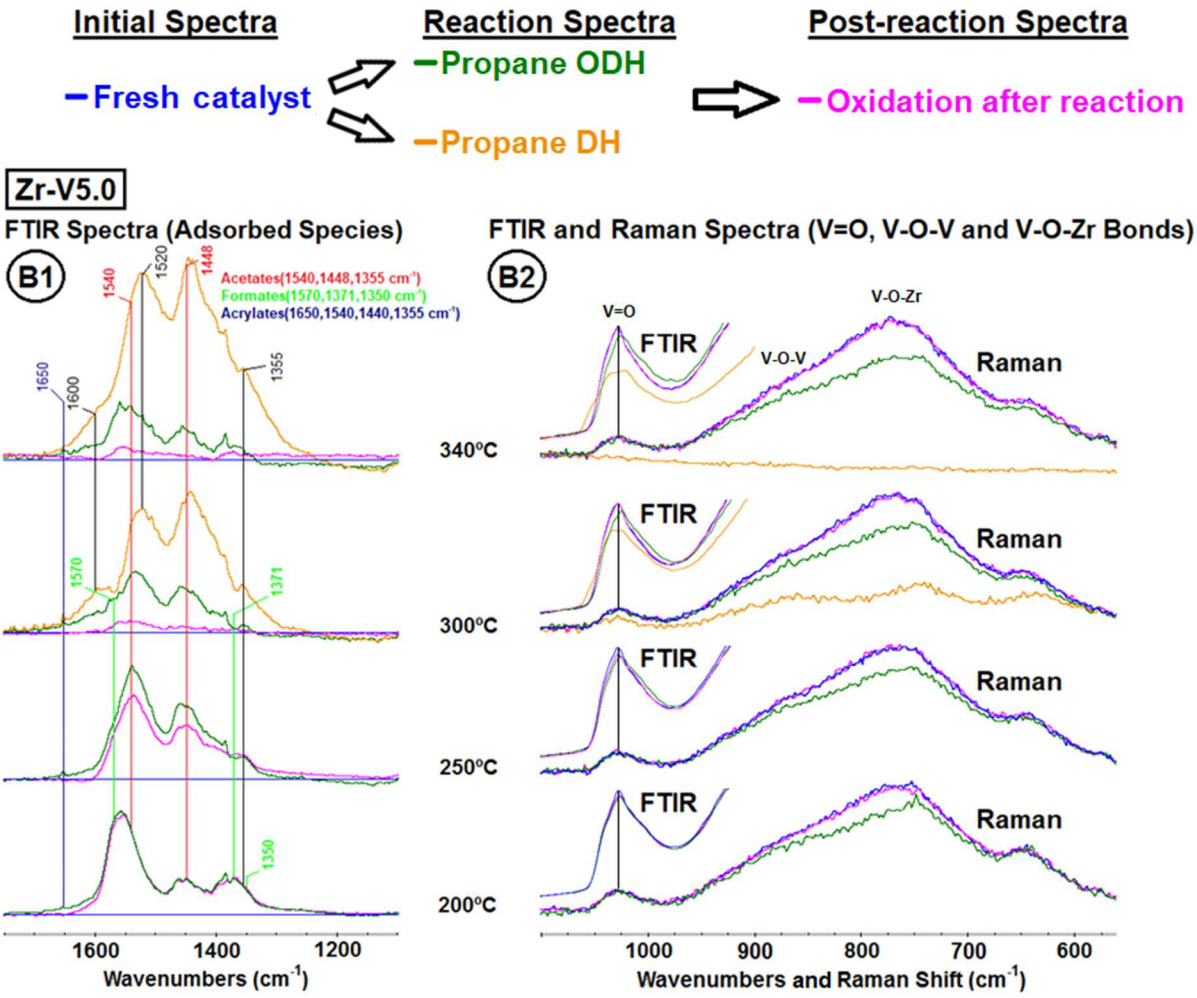
Initial Spectra
Reaction Spectra
Post-reaction Spectra
Fresh catalyst
Propane ODH
Propane DH
Oxidation after reaction
Zr-V5.0
FTIR Spectra (Adsorbed Species)
FTIR and Raman Spectra (V=O, V-O-V and V-O-Zr Bonds)
B1
B2
Acetates(1540,1448,1355 cm-1)
Formates(1570,1371,1350 cm-1)
Acrylates(1650,1540,1440,1355 cm-1)
1650
1600
1540
1520
1448
1355
1570
1371
1350
V=O
V-O-V
V-O-Zr
FTIR
Raman
340°C
300°C
250°C
200°C
1600
1400
1200
1000
900
800
700
600
Wavenumbers (cm-1)
Wavenumbers and Raman Shift (cm-1)

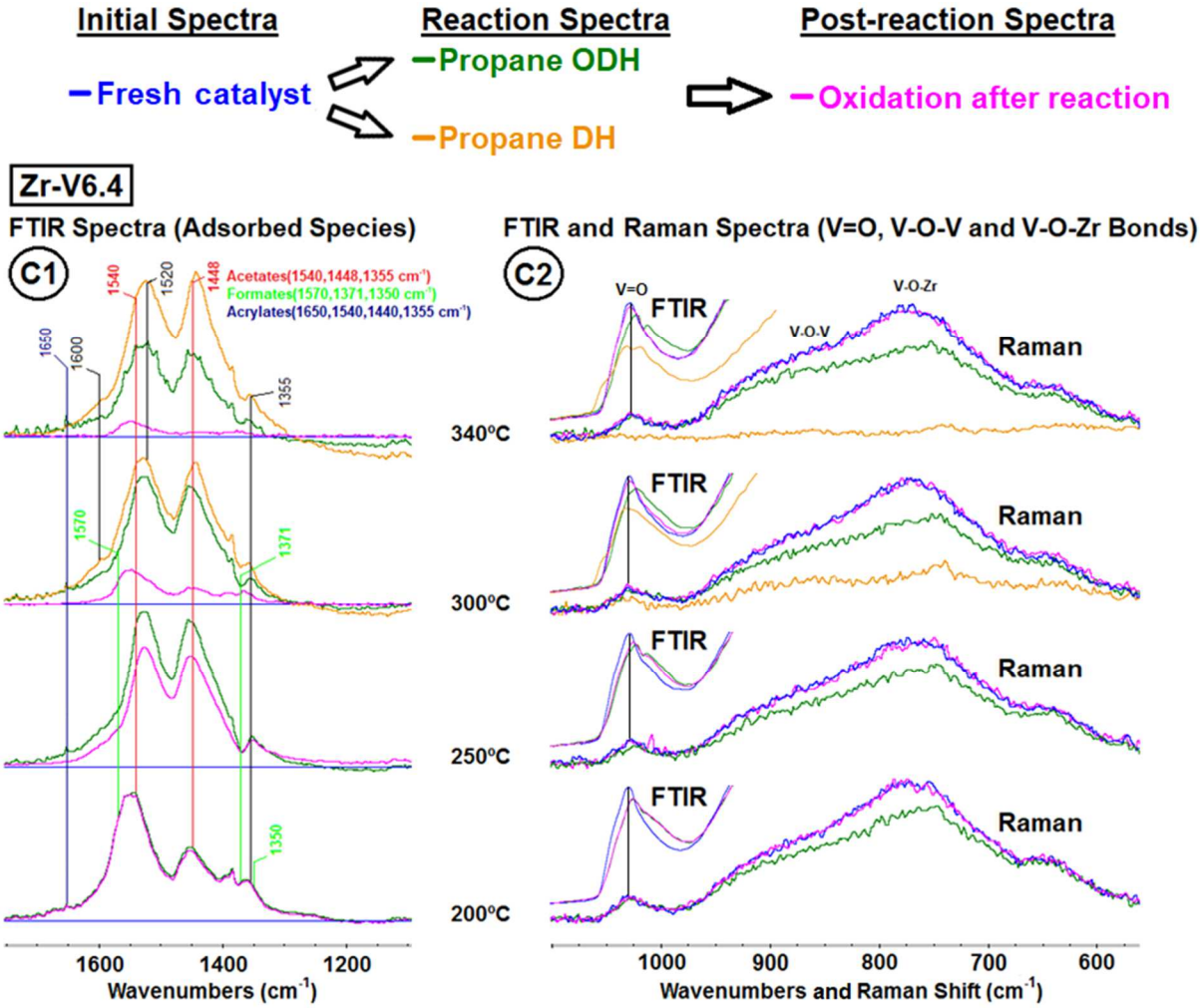

Figure 2. *Operando* FTIR (1 and 2) and Raman (2) spectra for Zr-V2.5 (A), Zr-V5.0 (B) and Zr-V6.4 (C). IR spectra shown at 1700-1100 cm^{-1} (1) were all subtracted with the reference spectrum of the fresh catalyst at the same temperature. Green and yellow traces represent ODH and DH experiments, respectively. Blue and pink traces represent oxidation experiments before and after reaction, respectively.

At 200ºC, despite negligible activity for ODH reaction (green trace), Zr-V5.0 and Zr-V6.4 exhibit stable infrared bands in the 1600-1300 cm^{-1} region (Figure 2 B1 and C1, respectively) that can be attributed to a mixture of bidentate acetates (1540, 1448, and 1355 cm^{-1}), acrylates (1640, 1540, 1440, and 1355 cm^{-1}) and bidentate formates (1570, 1371, and 1350 cm^{-1}) [17,87–91], which remain on the surface upon subsequent oxidation (pink trace). Infrared V=O mode redshifts (Figure 2 B2 and C2, respectively) can be observed during ODH (green traces) with respect to Zr-V5.0 and Zr-V6.4 dehydrated state (blue traces). The redshift is not reversed upon reoxidation (pink trace) at this temperature. The intensity of the V-O-V and V-O-Zr modes decreases during propane ODH (Fig. 2 A2, B2 and C2) (green traces) and is restored upon reoxidation (pink spectra).

At 250°C the catalytic activity is already apparent for Zr-V5.0 and Zr-V6.4 (Table 1), and the IR spectra show some differences in the region of adsorbed species. The acetate-to-formate ratio increase with temperature for both catalysts (Figure 2 B1 and C1) may be due to the lower thermal stability of formates [92]. In fact, only a slight removal of acetate species is achieved upon reoxidation at 250°C.

At higher temperatures (300 and 340ºC), the reaction rate becomes significantly higher (Table 1). Accordingly, the adsorbed oxygenates on Zr-V5.0 and Zr-V6.4 (Figure 2 B1 and C1) decrease significantly during ODH reaction (green spectra). The infrared V=O mode perturbation during ODH reaction (green traces in Figure 2 B2 and C2) is reversed upon reoxidation at these temperatures (pink spectra) along with the concomitant removal of the

oxygenate species (Figure 2 B1 and C1) and formation of gaseous CO_x and water.

In the case of Zr-V2.5, the position of the V=O band remains unchanged during ODH reaction and the intensity of the V-O-V and V-O-Zr modes is hardly recovered by reoxidation at the lower temperatures (Figure 2 A2). Zr-V2.5 is still apparently inactive at 250 ºC, but its features resemble those described above for Zr-V5.0 and Zr-V6.4 at 200ºC, with the development of a mixture of bidentate acetates, acrylates and bidentate formate species (Figure 2 A). Similarly, Zr-V2.5 spectra and activity at 300 and 340ºC are similar to those of Zr-V5.0 and Zr-V6.4 at 250 and 300ºC, respectively. The infrared spectra of Zr-V2.5 during reaction (green trace) show that surface acetate, acrylate and formate species hardly change.

The *operando* propane ODH data suggest that the catalysts are partly reduced or their polymerization decreases during reaction, and that between the detected acetate and formate intermediate species the latter decompose to CO faster, which is consistent with the higher stability of acetates with respect to formates [92]. As observed elsewhere [17,27,93], the formation of surface carbonates during the evolution of such carboxylate species to CO_x cannot be discarded. Moreover, the formation of other species than carboxylates cannot be excluded (e.g. intermediates for propylene formation) [40] at low or negligible surface concentrations that would not be detectable in these experiments. The slight perturbations of the V=O band could be associated with these adsorbed species, as the perturbations disappear when the oxygenates are removed, regardless of whether the catalyst has been reoxidized.

V=O and V-O-V/V-O-Zr bands show changes of position and intensity, respectively, during reaction, which are reversible upon reoxidation. The bridging V-O-V and V-O-Zr appear to interact with propane at lower temperatures than the terminal oxygens (200 ºC in Figure 2 A2), which indicates that bridging oxygens are more reactive than the oxo group, in agreement with previous works [42,52,67]. The increase of surface vanadium coverage leads to higher polyvanadates to monovanadates ratio and TOF values, suggesting that polyvanadates are more active than monovanadates.

3.2.2. Propane DH

Figure 2 also shows the *operando* spectra during DH reaction (yellow trace) at 300 and 340 ºC; DH data at 200 and 250 ºC show no appreciable difference with ODH data and thus are not shown. There is a higher surface concentration of adsorbed oxygenates during propane DH (Figure 2 A1, B1 and C1). Unlike propane ODH, where acetate and formate species are simultaneously formed and removed, during propane DH acetates dominate, with minor amounts of acrylates. Lattice oxygen is required for the evolution of acetate and acrylate species, with concomitant catalyst reduction, but not to decompose formates into CO [92,94]. The formation of carbonaceous deposits is evidenced by a shoulder around 1600 cm^{-1} in the FTIR spectra and around 1430 and 1600 cm^{-1} in the Raman spectra (Figure S2 in Supplementary information), with a concomitant decrease of V=O, V-O-V and V-O-Zr modes intensity (Figure 2 A2, B2 and C2) (yellow traces). As in ODH, vanadia bands are only restored upon reoxidation.

Figure 3 shows the spectra during *operando* propane DH on the Zr-V6.4 catalyst at 340ºC; fresh catalyst and propane ODH spectra at the same temperature are included as references in dark blue and dark green traces, respectively. The Raman acquisition time was reduced from 180 to 60 s to increase time resolution, which decreased the signal-to-noise ratio. Propylene, CO and CO_2 appear as initial gaseous products, which concentration decreases over time (Figure 3 B) as the lattice oxygen is consumed (Figure 3 C) and adsorbed species (mainly acetates) form (Figure 3 A). The detection of these products during several minutes in the absence of molecular oxygen confirms the participation of lattice oxygen, in line with a Mars-Van-Krevelen type mechanism [13].

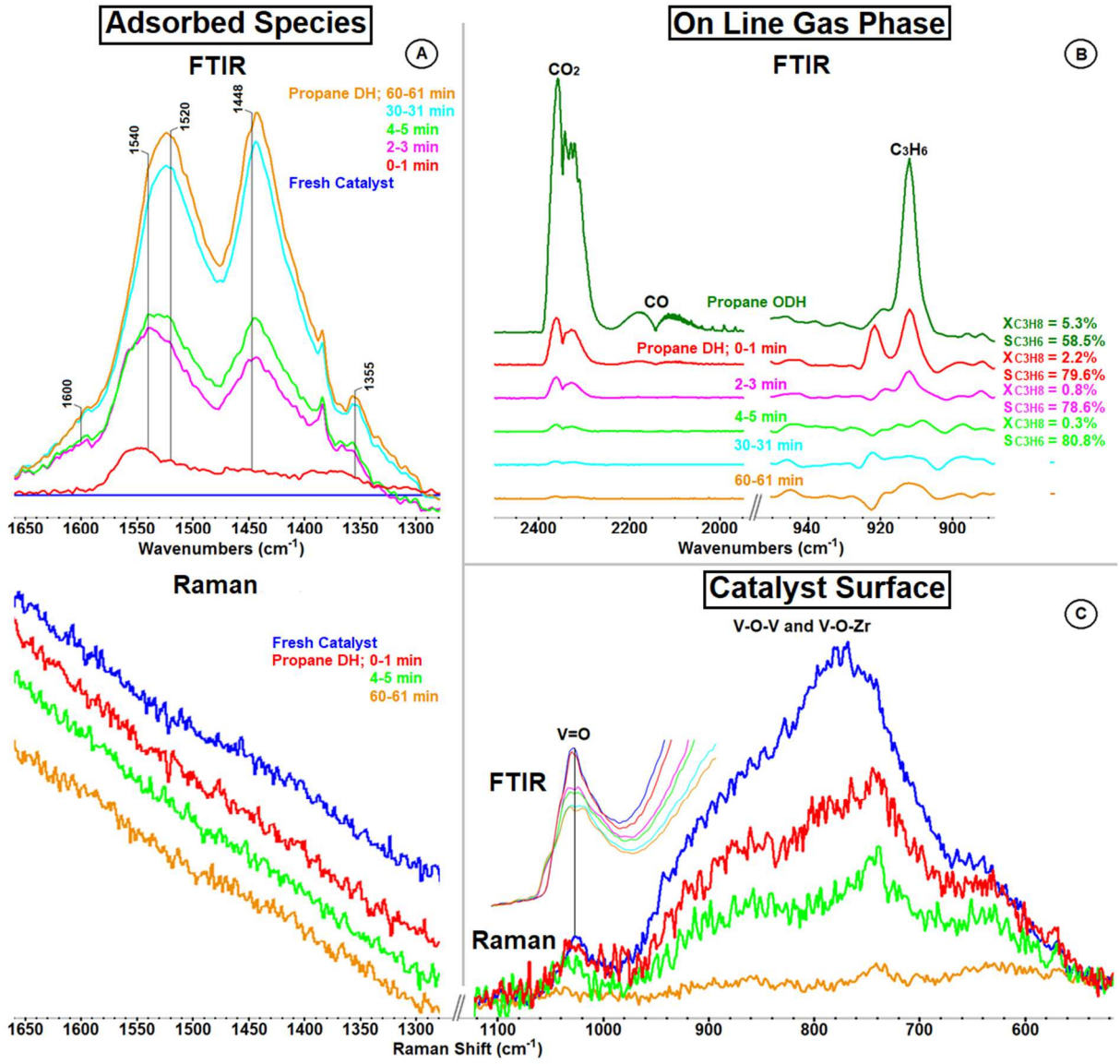

Figure 3. Evolution over time of the adsorbed species by FTIR (subtracted spectra) and Raman spectra (A), on line gas phase FTIR spectra including propane conversion and propylene selectivity values (B) and catalyst surface features in the FTIR and Raman spectra (C) of Zr-V6.4 during propane DH (20% C_3H_8 in Ar) at 340 ºC. The fresh catalyst (dark blue) and the ODH spectra (dark green) at the same temperature are included as reference.

As expected, propane DH conversion is lower than steady state ODH (Figure 3 B). DH propylene selectivity values are higher than steady state ODH. A significant intensity decrease of the Raman bands associated with V-O-V/V-O-Zr bonds is observed during the first minute of DH reaction (Figure 3 C, red vs. dark blue spectra); this shows a fast reduction at the bridging oxygen vanadium

sites, while the V=O sites hardly change (Figure 3 C). The activity slowly decreases with time on stream, being almost negligible after 3 minutes, while the lattice oxygen from V-O-V/V-O-Zr sites is further consumed. At this moment, the reduction of V=O sites becomes apparent, suggesting that terminal oxygen is much less active. Upon depletion of the catalyst reactive oxygen sites, acetate and acrylate species progressively accumulate on the surface, without significant formation of reaction products. The IR band by 1600 cm^{-1} after the first minute on stream evidences the formation of coke when the catalyst reduces (Figure 3 A). Finally, quasi-steady state of the catalyst is achieved after 60 minutes of propane DH. It should be noted the different sensibilities of the IR and Raman spectra in the range of the adsorbed species. While IR is more sensitive to oxygenated surface species, Raman is more sensitive to more polyolefinic species. Similar data during propane DH are reported in Figure S3 and S4 for Zr-V5.0 and Zr-V2.5, respectively, where the FTIR spectra display the features of acetate species and the Raman spectra evidence coke formation.

In summary*operando* DH results indicate that the V-O-V/V-O-Zr sites (lattice bridging oxygens) oxidize propane without the participation of gas phase oxygen, while the V=O site does not play a critical role. This is consistent with our conclusions and the literature [42,52,67,68], where V-O-V/V-O-Zr bonds are proposed as the active sites rather than the V=O bonds.

3.2.3. Propylene ODH

A propylene ODH experiment was also run (Figure 4). After activation at 340°C, propylene ODH feed was sent at room temperature to the IRRaman *operando* reactor that was subsequently heated to 100 ºC at 5 ºC·min^{-1}. After 48 min runtime the feed was switched to reoxidize the catalyst at 150°C until the spectra showed no appreciable changes. As shown in Figure 4 for Zr-V5.0, during propylene ODH some FTIR bands of physisorbed propylene appear at room temperature (1638, 1454, 1440, 1420 and 1372 cm^{-1}) [93]. Bands characteristic of adsorbed isopropoxide (1468, 1455, 1385, 1370, 1330, 1168, 1137 and 1115 cm^{-1}) and chemisorbed acetone (1682, 1421, 1368, 1245 and 1090 cm^{-1}) [87] become apparent at 100 ºC; these species are also visible at 150 ºC under the subsequent oxidation conditions, but the band of isopropoxide decreased as the band of acetone increased (dark blue trace) up to its maximum concentration, reached after 86 min. Thereafter, acetone started to decrease and new bands characteristic of bidentate acetates and bidentate formates developed, similarly to the propane ODH experiments (Figure 2 A1, B1 and C1).

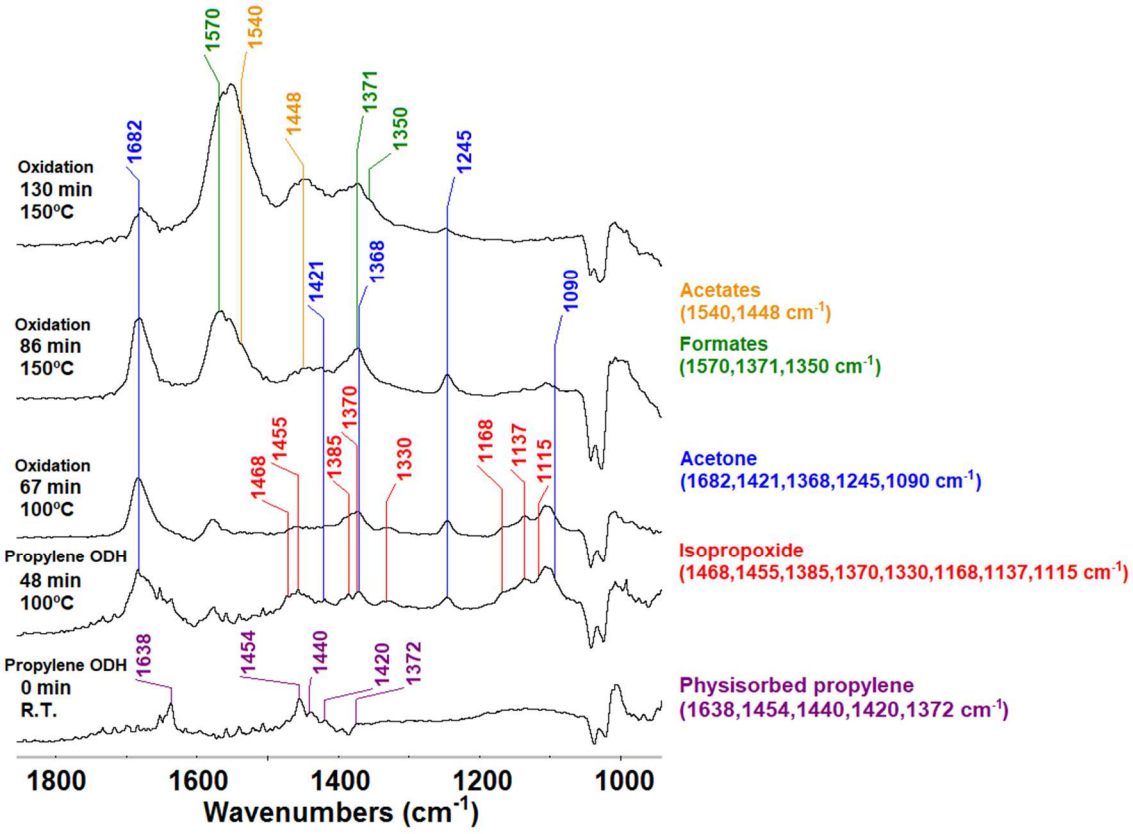

Figure 4. *Operando* FTIR spectra for Zr-V5.0 during propylene ODH reaction (20% C_3H_6 and 10% O_2 in Ar), and subsequent oxidation (10% O_2 in Ar).

3.3. *Proposed mechanism*

According to the *operando* experiments, both propane [24,27,5] and propylene [17,27,92,93,95,96] activation on V-Zr-O catalysts mainly proceed via isopropoxide species to form chemisorbed acetone and carboxylates, precursors of CO_x, unlike other studies that have reported the activation of propylene through allyl-alkoxides giving rise to chemisorbed acrolein and acrylates [24,38,92,93,96,97]. Therefore, a common surface intermediate is responsible of both propane and propylene ODH parallel reactions [27,98] and its consecutive oxidations eventually lead to the formation of CO_x total oxidation products. Scheme 2 illustrates the propane ODH mechanism derived from these experiments and assumptions.

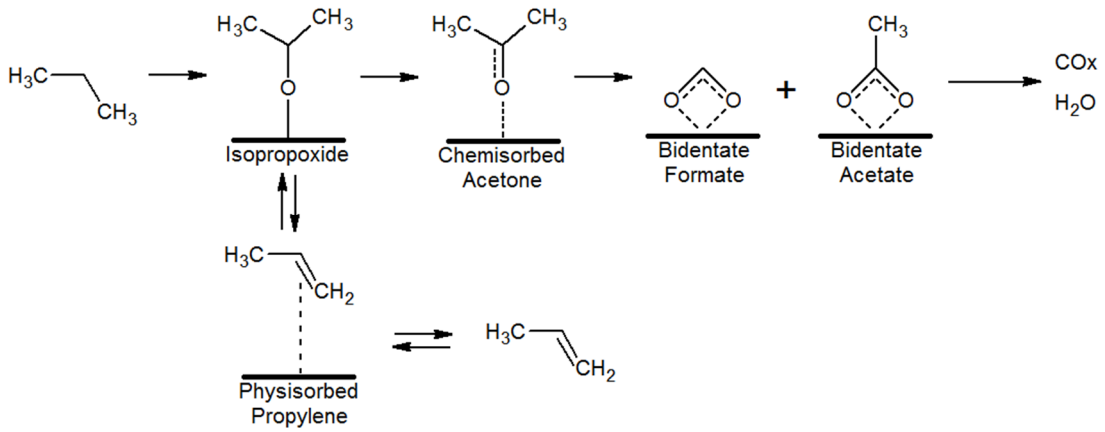

Scheme 2. Proposed mechanism derived from *operando* FTIR spectra obtained during propane/propylene partial oxidation reaction (ODH) and literature results.

Scheme 3 represents a proposed general mechanism consistent with current results, and in line with other works in the literature [5,17,25,27,93,95]. Our model assumes that only the lattice oxygen reacts with the adsorbed species, following a Mars-van-Krevelen type mechanism. The bridging lattice oxygen is represented as V-O-M, where M is V or Zr, assuming that both are active sites having the same role in the mechanism; the participation of V=O terminal oxygen is not considered. V-OH and V-□-M represent a protonated lattice oxygen and a vacancy site, respectively. It is proposed that propane oxidation occurs via the irreversible isopropoxide formation (R2), according to Iglesia *et al*. [25], which can give rise reversibly to propylene (R3.1) or be further oxidized to chemisorbed acetone (R3.2). The propylene formed can be released in the gas phase or adsorbed again on the surface and oxidized to isopropoxide species through a neighboring V-OH as Brønsted acidic site (R3.1.1 and R3.1, respectively), and continues with the subsequent oxidation steps (R3.2). Then, bidentate formates and acetates form by oxidative cleavage of the C(1)-C(2) bond of chemisorbed acetone (R4). These oxygenate species further evolve to CO (R5.1 and R5.2), but not to CO_2; this is in line with a previous work results

with the same catalysts [69]. CO could be released to the gas phase or be further oxidized to CO_2 (R6). The total oxidation through acrylates intermediates might be possible, and the formation of carbonate surface species cannot be discarded during the evolution of the carboxylates, as reported in other works [17,27,93], but these reactions were not included in the scheme. The equations R1 and R7 represent the catalyst reoxidation reactions, where the irreversible dissociative adsorption of gas-phase O_2 and the reversible OH recombination take place.

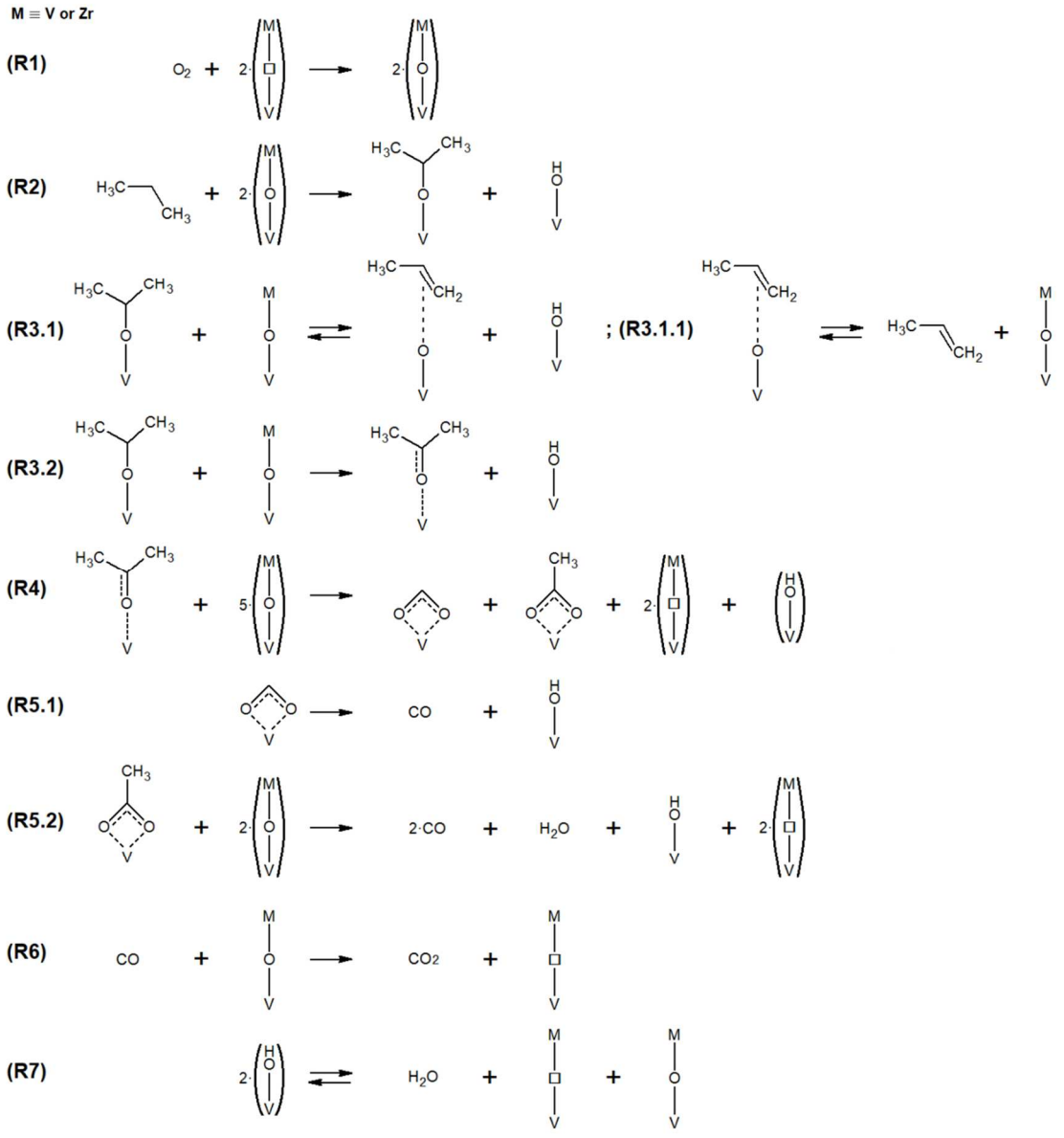

Scheme 3. Proposed detailed general mechanism based on the results obtained in this work and the literature about propane ODH [5,17,25,27,93,95]. V-O-M, V-□-M and V-OH represent lattice bridging oxygens, reduced vanadium sites and protonated lattice oxygens, respectively.

4. Conclusions

The new "IRRaman" multimodal *operando* reactor was used to study the structure-activity relationships of V-Zr-O catalysts during propane ODH; the simultaneous acquisition of activity data together with FTIR and Raman spectra of the working catalyst with space and time consistency has been decisive to gain insight about the propane ODH mechanism. The results indicate that the reaction occurs via a Mars-van-Krevelen type mechanism. Propane activation, the rate determining step, occurs through the formation of isopropoxide species, which may desorb as propylene or further oxidize to chemisorbed acetone. The latter would be converted into acetate and formate species; these carboxylates would be the precursors of CO_x. The propylene formed during reaction might react with a surface OH group as Brønsted acidic site to form isopropoxide species that would be further oxidized via the previously described pathway. It has been directly and unambiguously observed that the V-O-V/V-O-Zr sites are significantly more active than the terminal V=O bonds, clarifying the confusion created in literature. The results also show that polyvanadates present a slightly higher activity than monovanadates. Therefore, valuable information was obtained that lays the groundwork for future kinetic studies.

Acknowledgements

The authors acknowledge the FEDER-Region Basse-Normandie (France)-CNRS for a *Chaire d'Excellence* for MAB, which resulted in the implementation of the "IRRaman" rig and a research stay allowing to perform these

investigations. This work was also supported by the Spanish Ministry of Economy and Competitiveness and FEDER (CTQ2012-36408, CTQ2015-68654-R and CTM2017-82335-R). J.J.T.H. acknowledges the assistance of the Ministry of Economy and Competitiveness of Spain for the award of a FPI Grant (BES-2013-064425) and the award for performing his stay at LCS (EEBB-I-16-10749).

References

[1] R.H. Crabtree, Alkane C–H activation and functionalization with homogeneous transition metal catalysts: a century of progress—a new millennium in prospect, J. Chem. Soc. Dalton Trans. (2001) 2437–2450. https://doi.org/10.1039/B103147N.

[2] F. Cavani, J.H. Teles, Sustainability in Catalytic Oxidation: An Alternative Approach or a Structural Evolution?, ChemSusChem. 2 (2009) 508–534. https://doi.org/10.1002/cssc.200900020.

[3] F. Cavani, N. Ballarini, A. Cericola, Oxidative dehydrogenation of ethane and propane: How far from commercial implementation?, Catal. Today. 127 (2007) 113–131. https://doi.org/10.1016/j.cattod.2007.05.009.

[4] C.A. Carrero, R. Schloegl, I.E. Wachs, R. Schomaecker, Critical Literature Review of the Kinetics for the Oxidative Dehydrogenation of Propane over Well-Defined Supported Vanadium Oxide Catalysts, ACS Catal. 4 (2014) 3357–3380. https://doi.org/10.1021/cs5003417.

[5] R. Grabowski, Kinetics of oxidative dehydrogenation of C2-C3 alkanes on oxide catalysts, Catal. Rev. - Sci. Eng. 48 (2006) 199–268. https://doi.org/10.1080/01614940600631413.

[6] J. Lazonby, Propene (Propylene), (n.d.). http://www.essentialchemicalindustry.org/chemicals/propene.html (accessed April 2021).

[7] E.G. Rightor, C.L. Tway, Global energy & emissions reduction potential of chemical process improvements, Catal. Today 258 (2015) 226-229

[8] I. Amghizar, L.A. Vandewalle, G. Van, G.B. Marin, New Trends in Olefin Production, 3 (2017) 171–178. https://doi.org/10.1016/J.ENG.2017.02.006.

[9] A. Corma, J.M. López-Nieto, N. Paredes, M. Pérez, Y. Shen, H. Cao, S.L. Suib, Oxidative Dehydrogenation Of Propane Over Supported-Vanadium Oxide Catalysts, in: P. Ruiz, B. Delmon (Eds.), Stud. Surf. Sci. Catal., Elsevier, 1992: pp. 213–220. https://doi.org/10.1016/S0167-2991(08)61673-0.

[10] B. Frank, A. Dinse, O. Ovsitser, E.V. Kondratenko, R. Schomäcker, Mass and heat transfer effects on the oxidative dehydrogenation of propane (ODP) over a low loaded VOx/Al2O3 catalyst, Appl. Catal. Gen. 323 (2007) 66–76. https://doi.org/10.1016/j.apcata.2007.02.006.

[11] Y.-M. Liu, Y. Cao, K.-K. Zhu, S.-R. Yan, W.-L. Dai, H.-Y. He, K.-N. Fan, Highly efficient VOx/SBA-15 mesoporous catalysts for oxidative

dehydrogenation of propane, Chem. Commun. 0 (2002) 2832–2833. https://doi.org/10.1039/B208177F.
[12] Y.-M. Liu, Y. Cao, N. Yi, W.-L. Feng, W.-L. Dai, S.-R. Yan, H.-Y. He, K.-N. Fan, Vanadium oxide supported on mesoporous SBA-15 as highly selective catalysts in the oxidative dehydrogenation of propane, J. Catal. 224 (2004) 417–428. https://doi.org/10.1016/j.jcat.2004.03.010.
[13] P. Mars, D.W. van Krevelen, Oxidations carried out by means of vanadium oxide catalysts, Chem. Eng. Sci. 3 (1954) 41–59. https://doi.org/10.1016/S0009-2509(54)80005-4.
[14] E.V. Kondratenko, M. Cherian, M. Baerns, D. Su, R. Schlögl, X. Wang, I.E. Wachs, Oxidative dehydrogenation of propane over V/MCM-41 catalysts: comparison of O2 and N2O as oxidants, J. Catal. 234 (2005) 131–142. https://doi.org/10.1016/j.jcat.2005.05.025.
[15] A. Dinse, B. Frank, C. Hess, D. Habel, R. Schomäcker, Oxidative dehydrogenation of propane over low-loaded vanadia catalysts: Impact of the support material on kinetics and selectivity, J. Mol. Catal. Chem. 289 (2008) 28–37. https://doi.org/10.1016/j.molcata.2008.04.007.
[16] B.Y. Jibril, S.M. Al-Zahrani, A.E. Abasaeed, R. Hughes, Propane oxidative dehydrogenation on Cs-doped Cr-Mo-Al-O catalyst: kinetics and mechanism, Chem. Eng. J. 103 (2004) 59–67. https://doi.org/10.1016/j.cej.2004.03.006.
[17] M. Baldi, E. Finocchio, C. Pistarino, G. Busca, Evaluation of the mechanism of the oxy-dehydrogenation of propane over manganese oxide, Appl. Catal. Gen. 173 (1998) 61–74. https://doi.org/10.1016/S0926-860X(98)00129-X.
[18] K. Routray, K.R.S.K. Reddy, G. Deo, Oxidative dehydrogenation of propane on V2O5/Al2O3 and V2O5/TiO2 catalysts: understanding the effect of support by parameter estimation, Appl. Catal. Gen. 265 (2004) 103–113. https://doi.org/10.1016/j.apcata.2004.01.006.
[19] S. Chakraborty, S.C. Nayak, G. Deo, TiO2/SiO2 supported vanadia catalysts for the ODH of propane, Catal. Today. 254 (2015) 62–71. https://doi.org/10.1016/j.cattod.2015.01.047.
[20] E.V. Kondratenko, M. Baerns, Catalytic oxidative dehydrogenation of propane in the presence of O2 and N2O—the role of vanadia distribution and oxidant activation, Appl. Catal. Gen. 222 (2001) 133–143. https://doi.org/10.1016/S0926-860X(01)00836-5.
[21] T. Blasco, J.M.L. Nieto, Oxidative dyhydrogenation of short chain alkanes on supported vanadium oxide catalysts, Appl. Catal. Gen. 157 (1997) 117–142. https://doi.org/10.1016/S0926-860X(97)00029-X.
[22] A. Dinse, S. Khennache, B. Frank, C. Hess, R. Herbert, S. Wrabetz, R. Schlögl, R. Schomäcker, Oxidative dehydrogenation of propane on silica (SBA-15) supported vanadia catalysts: A kinetic investigation, J. Mol. Catal. Chem. 307 (2009) 43–50. https://doi.org/10.1016/j.molcata.2009.03.008.
[23] H.H. Kung, Oxidative Dehydrogenation of Light (C2 to C4) Alkanes, in: D.D. Eley, H. Pines, W.O. Haag (Eds.), Adv. Catal., Academic Press, 1994: pp. 1–38. https://doi.org/10.1016/S0360-0564(08)60655-0.
[24] K. Chen, A.T. Bell, E. Iglesia, Kinetics and Mechanism of Oxidative Dehydrogenation of Propane on Vanadium, Molybdenum, and Tungsten Oxides, J. Phys. Chem. B. 104 (2000) 1292–1299. https://doi.org/10.1021/jp9933875.

[25] K. Chen, A. Khodakov, J. Yang, A.T. Bell, E. Iglesia, Isotopic Tracer and Kinetic Studies of Oxidative Dehydrogenation Pathways on Vanadium Oxide Catalysts, J. Catal. 186 (1999) 325–333. https://doi.org/10.1006/jcat.1999.2510.
[26] M.O. Guerrero-Pérez, A.J. McCue, J.A. Anderson, Rapid scan FTIR reveals propane (am)oxidation mechanisms over vanadium based catalysts, J. Catal. 390 (2020) 72–80. https://doi.org/10.1016/j.jcat.2020.07.031.
[27] G. Busca, E. Finocchio, V. Lorenzelli, G. Ramis, M. Baldi, IR studies on the activation of C–H hydrocarbon bonds on oxidation catalysts, Catal. Today. 49 (1999) 453–465. https://doi.org/10.1016/S0920-5861(98)00441-6.
[28] A.S. Sandupatla, S.C. Nayak, C. Sivananda, G. Deo, DFT investigation into the experimentally observed influence of oxide support in the ODH of propane over supported vanadia catalysts, Catal. Today. (2019). https://doi.org/10.1016/j.cattod.2018.05.058.
[29] K. Tarama, S. Yoshida, S. Ishida, H. Kakioka, Spectroscopic Studies of Catalysis by Vanadium Pentoxide, Bull. Chem. Soc. Jpn. 41 (1968) 2840–2845. https://doi.org/10.1246/bcsj.41.2840.
[30] K. Mori, A. Miyamoto, Y. Murakami, Catalytic reactions on well-characterized vanadium oxide catalysts. 4. Oxidation of butane, J. Phys. Chem. 89 (1985) 4265–4269. https://doi.org/10.1021/j100266a024.
[31] S.T. Oyama, Adsorbate bonding and the selection of partial and total oxidation pathways, J. Catal. 128 (1991) 210–217. https://doi.org/10.1016/0021-9517(91)90078-I.
[32] A. Andersson, An oxidized surface state model of vanadium oxides and its application to catalysis, J. Solid State Chem. 42 (1982) 263–275. https://doi.org/10.1016/0022-4596(82)90005-6.
[33] F. Gilardoni, A.T. Bell, A. Chakraborty, P. Boulet, Density functional theory calculations of the oxidative dehydrogenation of propane on the (010) surface of C2O5, J. Phys. Chem. B. 104 (2000) 12250–12255.
[34] H. Fu, Z.-P. Liu, Z.-H. Li, W.-N. Wang, K.-N. Fan, Periodic Density Functional Theory Study of Propane Oxidative Dehydrogenation over V2O5(001) Surface, J. Am. Chem. Soc. 128 (2006) 11114–11123. https://doi.org/10.1021/ja0611745.
[35] M.-J. Cheng, K. Chenoweth, J. Oxgaard, A. van Duin, W.A. Goddard, Single-Site Vanadyl Activation, Functionalization, and Reoxidation Reaction Mechanism for Propane Oxidative Dehydrogenation on the Cubic V4O10 Cluster, J. Phys. Chem. C. 111 (2007) 5115–5127. https://doi.org/10.1021/jp0663917.
[36] K. Alexopoulos, M.-F. Reyniers, G.B. Marin, Reaction path analysis of propane selective oxidation over V2O5 and V2O5/TiO2, J. Catal. 289 (2012) 127–139. https://doi.org/10.1016/j.jcat.2012.01.019.
[37] C. Xiong, S. Chen, P. Yang, S. Zha, Z.-J. Zhao, J. Gong, Structure-Performance Relationships for Propane Dehydrogenation over Aluminum Supported Vanadium Oxide, ACS Catal. 9 (2019) 5816–5827. https://doi.org/10.1021/acscatal.8b04701.
[38] C. Zhao, I.E. Wachs, An Operando Raman, IR, and TPSR Spectroscopic Investigation of the Selective Oxidation of Propylene to Acrolein over a Model Supported Vanadium Oxide Monolayer Catalyst, J. Phys. Chem. C. 112 (2008) 11363–11372. https://doi.org/10.1021/jp801562g.

[39] A. Christodoulakis, M. Machli, A.A. Lemonidou, S. Boghosian, Molecular structure and reactivity of vanadia-based catalysts for propane oxidative dehydrogenation studied by in situ Raman spectroscopy and catalytic activity measurements, J. Catal. 222 (2004) 293–306. https://doi.org/10.1016/j.jcat.2003.10.007.
[40] M.O. Guerrero-Pérez, Supported, bulk and bulk-supported vanadium oxide catalysts: A short review with an historical perspective, Catal. Today. 285 (2017) 226–233. https://doi.org/10.1016/j.cattod.2017.01.037.
[41] P.M. Michalakos, M.C. Kung, I. Jahan, H. Kung, Selectivity Patterns in Alkane Oxidation over Mg3(VO4)2-MgO, Mg2V2O7, and (VO)2P2O7, J. Catal. 140 (1993) 226–242. https://doi.org/10.1006/jcat.1993.1080.
[42] J.G. Eon, R. Olier, J.C. Volta, Oxidative Dehydrogenation of Propane on γ-Al2O3 Supported Vanadium Oxides, J. Catal. 145 (1994) 318–326. https://doi.org/10.1006/jcat.1994.1040.
[43] A.D. Costa, C. Mathieu, Y. Barbaux, H. Poelman, G. Dalmai-Vennik, L. Fiermans, Observation of the V2O5(001) surface using ambient atomic force microscopy, Surf. Sci. 370 (1997) 339–344. https://doi.org/10.1016/S0039-6028(96)00956-9.
[44] J. Sambeth, A. Juan, L. Gambaro, H. Thomas, Catalytic oxidation of CH3OH to HCOOCH3 on V2O5: A theoretical study, J. Mol. Catal. Chem. 118 (1997) 283–291. https://doi.org/10.1016/S1381-1169(96)00900-4.
[45] A. Kämper, A. Auroux, M. Baerns, A molecular mechanics study of the adsorption of ethane and propane on a V2O5(001) surface, Phys. Chem. Chem. Phys. 2 (2000) 1069–1075. https://doi.org/10.1039/A908988H.
[46] A. Kämper, I. Hahndorf, M. Baerns, A molecular mechanics study of the adsorption of ethane and propane on V2O5(001) surfaces with oxygen vacancies, Top. Catal. 11 (2000) 77–84. https://doi.org/10.1023/A:1027239612464.
[47] M.V. Martínez-Huerta, G. Deo, J.L.G. Fierro, M.A. Bañares, Operando Raman-GC Study on the Structure–Activity Relationships in V 5+/CeO 2 Catalyst for Ethane Oxidative Dehydrogenation: The Formation of CeVO 4, J. Phys. Chem. C. 112 (2008) 11441–11447. https://doi.org/10.1021/jp802827t.
[48] M. Witko, Quantum-chemical description of the active sites for the selective oxidation of hydrocarbons, Catal. Today. 32 (1996) 89–95. https://doi.org/10.1016/S0920-5861(96)00187-3.
[49] M. Witko, R. Tokarz, J. Haber, Vanadium pentoxide. II. Quantum chemical modeling, Appl. Catal. Gen. 157 (1997) 23–44. https://doi.org/10.1016/S0926-860X(97)00019-7.
[50] A. Michalak, M. Witko, K. Hermann, Density functional cluster studies on the (010) surface of vanadium pentoxide, Surf. Sci. 375 (1997) 385–394. https://doi.org/10.1016/S0039-6028(96)01286-1.
[51] M. Witko, K. Hermann, R. Tokarz, Adsorption and reactions at the (010) V2O5 surface: cluster model studies, Catal. Today. 50 (1999) 553–565. https://doi.org/10.1016/S0920-5861(98)00490-8.
[52] G. Deo, I.E. Wachs, Surface oxide-support interaction (SOSI) for surface redox sites, J. Catal. 129 (1991) 307–312. https://doi.org/10.1016/0021-9517(91)90036-4.

[53] G. Deo, I.E. Wachs, Reactivity of Supported Vanadium Oxide Catalysts: The Partial Oxidation of Methanol, J. Catal. 146 (1994) 323–334. https://doi.org/10.1006/jcat.1994.1071.
[54] I.E. Wachs, J.-M. Jehng, G. Deo, B.M. Weckhuysen, V.V. Guliants, J.B. Benziger, S. Sundaresan, Fundamental Studies of Butane Oxidation over Model-Supported Vanadium Oxide Catalysts: Molecular Structure-Reactivity Relationships, J. Catal. 170 (1997) 75–88. https://doi.org/10.1006/jcat.1997.1742.
[55] I.E. Wachs, B.M. Weckhuysen, Structure and reactivity of surface vanadium oxide species on oxide supports, Appl. Catal. Gen. 157 (1997) 67–90. https://doi.org/10.1016/S0926-860X(97)00021-5.
[56] L.J. Burcham, G. Deo, X. Gao, I.E. Wachs, In situ IR, Raman, and UV-Vis DRS spectroscopy of supported vanadium oxide catalysts during methanol oxidation, Top. Catal. 11 (2000) 85–100. https://doi.org/10.1023/A:1027275225668.
[57] M.A. Bañares, M. Martínez-Huerta, X. Gao, I.E. Wachs, J.L.G. Fierro, Identification and roles of the different active sites in supported vanadia catalysts by in situ techniques, in: A. Corma, F.V. Melo, S. Mendioroz, J.L.G. Fierro (Eds.), Stud. Surf. Sci. Catal., Elsevier, 2000: pp. 3125–3130. https://doi.org/10.1016/S0167-2991(00)80502-9.
[58] M.A. Bañares, I.E. Wachs, Molecular structures of supported metal oxide catalysts under different environments, J. Raman Spectrosc. 33 (2002) 359–380. https://doi.org/10.1002/jrs.866.
[59] X. Gao, J.-M. Jehng, I.E. Wachs, In Situ UV–vis–NIR Diffuse Reflectance and Raman Spectroscopic Studies of Propane Oxidation over ZrO2-Supported Vanadium Oxide Catalysts, J. Catal. 209 (2002) 43–50. https://doi.org/10.1006/jcat.2002.3635.
[60] I.E. Wachs, Recent conceptual advances in the catalysis science of mixed metal oxide catalytic materials, Catal. Today. 100 (2005) 79–94. https://doi.org/10.1016/j.cattod.2004.12.019.
[61] H. Tian, E.I. Ross, I.E. Wachs, Quantitative Determination of the Speciation of Surface Vanadium Oxides and Their Catalytic Activity, J. Phys. Chem. B. 110 (2006) 9593–9600. https://doi.org/10.1021/jp055767y.
[62] C. Zhao, I.E. Wachs, Selective oxidation of propylene over model supported V2O5 catalysts: Influence of surface vanadia coverage and oxide support, J. Catal. 257 (2008) 181–189. https://doi.org/10.1016/j.jcat.2008.04.022.
[63] I.E. Wachs, M. Bañares, In Situ and Operando Raman Spectroscopy of Oxidation Catalysts, in: Handb. Adv. Methods Process. Oxid. Catal., IMPERIAL COLLEGE PRESS, 2011: pp. 420–446. https://doi.org/10.1142/9781848167513_0017.
[64] I.E. Wachs, Catalysis science of supported vanadium oxide catalysts, Dalton Trans. 42 (2013) 11762–11769. https://doi.org/10.1039/C3DT50692D.
[65] I.E. Wachs, C.J. Keturakis, 7.06 - Monolayer Systems, in: J. Reedijk, K. Poeppelmeier (Eds.), Compr. Inorg. Chem. II Second Ed., Elsevier, Amsterdam, 2013: pp. 131–151. https://doi.org/10.1016/B978-0-08-097774-4.00717-8.
[66] M.A. Bañares, X. Gao, J.L.G. Fierro, I.E. Wachs, Partial oxidation of ethane over monolayers of vanadium oxide. effect of the support and

surface coverage, in: R.K. Grasselli, S.T. Oyama, A.M. Gaffney, J.E. Lyons (Eds.), Stud. Surf. Sci. Catal., Elsevier, 1997: pp. 295–304. https://doi.org/10.1016/S0167-2991(97)80990-1.
[67] A.E. Lewandowska, M. Calatayud, E. Lozano-Diz, C. Minot, M.A. Bañares, Combining theoretical description with experimental in situ studies on the effect of alkali additives on the structure and reactivity of vanadium oxide supported catalysts, Catal. Today. 139 (2008) 209–213. https://doi.org/10.1016/j.cattod.2008.04.049.
[68] J.J. Ternero-Hidalgo, M.O. Guerrero-Pérez, J. Rodríguez-Mirasol, T. Cordero, M.A. Bañares, R. Portela, P. Bazin, G. Clet, M. Daturi, Operando Reactor-Cell with Simultaneous Transmission FTIR and Raman Characterization (IRRaman) for the Study of Gas-Phase Reactions with Solid Catalysts, Anal. Chem. 92 (2020) 5100–5106. https://doi.org/10.1021/acs.analchem.9b05473.
[69] J.J. Ternero-Hidalgo, J. Torres-Liñán, M.O. Guerrero-Pérez, J. Rodríguez-Mirasol, T. Cordero, Electrospun vanadium oxide based submicron diameter fiber catalysts. Part I: Preparation procedure and propane ODH application, Catal. Today. 325 (2018) 131–143. https://doi.org/10.1016/j.cattod.2018.10.073.
[70] J.J. Ternero-Hidalgo, M.O. Guerrero-Pérez, J. Rodríguez-Mirasol, T. Cordero, Electrospun vanadium oxide based submicron diameter fiber catalysts. Part II: Effect of chemical formulation and dopants, Catal. Today. 325 (2018) 144–150. https://doi.org/10.1016/j.cattod.2018.10.072.
[71] S. Wuttke, P. Bazin, A. Vimont, C. Serre, Y.-K. Seo, Y.K. Hwang, J.-S. Chang, G. Férey, M. Daturi, Discovering the Active Sites for C3 Separation in MIL-100(Fe) by Using Operando IR Spectroscopy, Chem. – Eur. J. 18 (2012) 11959–11967. https://doi.org/10.1002/chem.201201006.
[72] S. Thomas, O. Marie, P. Bazin, L. Lietti, C.G. Visconti, M. Corbetta, F. Manenti, M. Daturi, Modelling a reactor cell for operando IR studies: From qualitative to fully quantitative kinetic investigations, Catal. Today. 283 (2017) 176–184. https://doi.org/10.1016/j.cattod.2016.07.008.
[73] S.B. Rasmussen, S. Perez-Ferreras, M.A. Bañares, P. Bazin, M. Daturi, Does pelletizing catalysts influence the efficiency number of activity measurements? Spectrochemical engineering considerations for an accurate operando study, ACS Catal. 3(1) (2013) 86–94. https://doi.org/10.1021/cs300687v.
[74] C.L. Pieck, S. del Val, M. López Granados, M.A. Bañares, J.L.G. Fierro, Bulk and Surface Structures of V2O5/ZrO2 Systems and Their Relevance for o-Xylene Oxidation, Langmuir. 18 (2002) 2642–2648. https://doi.org/10.1021/la0114631.
[75] S.A. D'Ippolito, M.A. Bañares, J.L.G. Fierro, C.L. Pieck, Propane Oxidative Dehydrogenation on V–Sb/ZrO2 Catalysts, Catal. Lett. 122 (2008) 252–258. https://doi.org/10.1007/s10562-008-9437-1.
[76] C.L. Pieck, M.A. Bañares, M.A. Vicente, J.L.G. Fierro, Chemical Structures of ZrO2-Supported V–Sb Oxides, Chem. Mater. 13 (2001) 1174–1180. https://doi.org/10.1021/cm000333v.
[77] M.O. Guerrero-Pérez, J.L.G. Fierro, M.A. Vicente, M.A. Bañares, Effect of Sb/V ratio and of Sb + V coverage on the molecular structure and activity of alumina-supported Sb-V-O catalysts for the ammoxidation of propane to

acrylonitrile, J. Catal. 206 (2002) 339–348. https://doi.org/10.1006/jcat.2001.3494.
[78] L. Fernandez, E. Sanchez, M. Panizza, M.M. Carnasciali, G. Busca, Vibrational and electronic spectroscopic properties of zirconia powders, J. Mater. Chem. 11 (2001) 1891–1897. https://doi.org/10.1039/b100909p.
[79] B.Y. Zhao, X.P. Xu, H.R. Ma, D.H. Sun, J.M. Gao, Monolayer dispersion of oxides and salts on surface of ZrO2 and its application in preparation of ZrO2-supported catalysts with high surface areas, Catal. Lett. 45 (1997) 237–244.
[80] E. Hryha, E. Rutqvist, L. Nyborg, Stoichiometric vanadium oxides studied by XPS, Surf. Interface Anal. 44(8) (2012) 1022–1025. https://doi.org/10.1002/sia.3844.
[81] D. Eisenbach, E. Gallei, Infrared spectroscopic investigations relating to coke formation on zeolites: I. Adsorption of hexene-1 and n-hexane on zeolites of type Y, J. Catal. 56 (1979) 377–389. https://doi.org/10.1016/0021-9517(79)90130-1.
[82] J. Datka, Z. Sarbak, R.P. Eischens, Infrared Study of Coke on Alumina and Zeolite, J. Catal. 145 (1994) 544–550. https://doi.org/10.1006/jcat.1994.1065.
[83] M. Daturi, C. Binet, J.C. Lavalley, G. Blanchard, Surface FTIR investigations on CexZr1−xO2 system, Surf. Interface Anal. 30 (2000) 273–277. https://doi.org/10.1002/1096-9918(200008)30:1<273::AID-SIA715>3.0.CO;2-G.
[84] K.K. Bando, K. Sayama, H. Kusama, K. Okabe, H. Arakawa, In-situ FT-IR study on CO2 hydrogenation over Cu catalysts supported on SiO2, Al2O3, and TiO2, Appl. Catal. Gen. 165 (1997) 391–409. https://doi.org/10.1016/S0926-860X(97)00221-4.
[85] G. Ramis, G. Busca, V. Lorenzelli, Low-temperature CO2 adsorption on metal oxides: spectroscopic characterization of some weakly adsorbed species, Mater. Chem. Phys. 29 (1991) 425–435. https://doi.org/10.1016/0254-0584(91)90037-U.
[86] I.E. Wachs, Raman and IR studies of surface metal oxide species on oxide supports: Supported metal oxide catalysts, Catal. Today. 27 (1996) 437–455. https://doi.org/10.1016/0920-5861(95)00203-0.
[87] Vicente. Sanchez Escribano, Guido. Busca, Vincenzo. Lorenzelli, Fourier transform infrared spectroscopic studies of the reactivity of vanadia-titania catalysts toward olefins. 1. Propylene, J. Phys. Chem. 94 (1990) 8939–8945. https://doi.org/10.1021/j100389a017.
[88] M. El-Roz, P. Bazin, M. Daturi, F. Thibault-Starzyk, Operando Infrared (IR) Coupled to Steady-State Isotopic Transient Kinetic Analysis (SSITKA) for Photocatalysis: Reactivity and Mechanistic Studies, ACS Catal. 3 (2013) 2790–2798. https://doi.org/10.1021/cs4006088.
[89] N.W. Alcock, V.M. Tracy, T.C. Waddington, Acetates and acetato-complexes. Part 2. Spectroscopic studies, J. Chem. Soc. Dalton Trans. 0 (1976) 2243–2246. https://doi.org/10.1039/DT9760002243.
[90] S.E. Collins, M.A. Baltanás, A.L. Bonivardi, An infrared study of the intermediates of methanol synthesis from carbon dioxide over Pd/β-Ga2O3, J. Catal. 226 (2004) 410–421. https://doi.org/10.1016/j.jcat.2004.06.012.

[91] Anatoli Davydov, Molecular Spectroscopy of Oxide Catalyst Surfaces, Wiley, 2003.
[92] E. Finocchio, G. Busca, V. Lorenzelli, V.S. Escribano, FTIR studies on the selective oxidation and combustion of light hydrocarbons at metal oxide surfaces. Part 2.—Propane and propene oxidation on Co3O4, J. Chem. Soc. Faraday Trans. 92 (1996) 1587–1593. https://doi.org/10.1039/FT9969201587.
[93] E. Finocchio, G. Busca, V. Lorenzelli, R.J. Willey, FTIR studies on the selective oxidation and combustion of light hydrocarbns at metal oxide surfaces. Propane and propene oxidation on MgCr2O4, J. Chem. Soc. Faraday Trans. 90 (1994) 3347–3356. https://doi.org/10.1039/FT9949003347.
[94] Vicente. Sanchez Escribano, Guido. Busca, Vincenzo. Lorenzelli, Fourier transform infrared spectroscopic studies of the reactivity of vanadia-titania catalysts toward olefins. 2. Ethylene, J. Phys. Chem. 94 (1990) 8945–8950. https://doi.org/10.1021/j100389a018.
[95] E. Finocchio, R.J. Willey, G. Ramis, G. Busca, V. Lorenzelli, Hydrocarbon activation and oxidation on transition metal mixed oxides: Ft-IR and flow reactor studies, in: J.W. Hightower, W. Nicholas Delgass, E. Iglesia, A.T. Bell (Eds.), Stud. Surf. Sci. Catal., Elsevier, 1996: pp. 483–492. https://doi.org/10.1016/S0167-2991(96)80259-X.
[96] E. Finocchio, R.J. Willey, G. Busca, V. Lorenzelli, FTIR studies on the selective oxidation and combustion oflight hydrocarbons at metal oxide surfaces Part3.—Comparison of the oxidation ofC3 organic compounds over Co3O4,MgCr2O4 and CuO, J. Chem. Soc. Faraday Trans. 93 (1997) 175–180. https://doi.org/10.1039/A605341F.
[97] C. Zhao, I.E. Wachs, Selective oxidation of propylene to acrolein over supported V2O5/Nb2O5 catalysts: An in situ Raman, IR, TPSR and kinetic study, Catal. Today. 118 (2006) 332–343. https://doi.org/10.1016/j.cattod.2006.07.018.
[98] E.A. Mamedov, V. Cortés Corberán, Oxidative dehydrogenation of lower alkanes on vanadium oxide-based catalysts. The present state of the art and outlooks, Appl. Catal. Gen. 127 (1995) 1–40. https://doi.org/10.1016/0926-860X(95)00056-9.

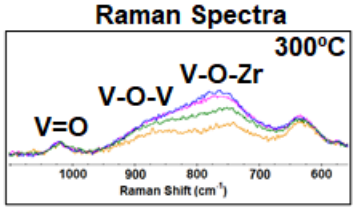

Catalytic Activity:
V-O-M >> V=O

Gas Phase

H_3C-CH_3

H_3C CH_2

COx + H_2O

MS & FTIR

Raman

IR

H_3C CH_3 O

CH_3

Backscattering

Transmission

Catalyst

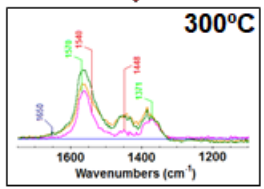

FTIR Spectra